A&A 437, 849–859 (2005)
DOI: 10.1051/0004-6361:20041945

Astronomy & Astrophysics

Spectroscopic study of blue compact galaxies

V. Oxygen abundance and the metallicity-luminosity relation

F. Shi[1], X. Kong[1,2], C. Li[1], and F. Z. Cheng[1]

[1] Center for Astrophysics, University of Science and Technology of China, 230026, PR China
e-mail: sfemail@mail.ustc.edu.cn;xkong@ustc.edu.cn
[2] National Astronomical Observatory, 2-21-1 Osawa, Mitaka, Tokyo 181-8588, Japan

Received 3 September 2004 / Accepted 14 March 2005

Abstract. This is the fifth paper in a series studying the stellar components, star formation histories, star formation rates and metallicities of a blue compact galaxy (BCG) sample. Based on our high-quality ground-based spectroscopic observations, we have determined the electron temperatures, electron densities, nitrogen abundances and oxygen abundances for 72 star-forming BCGs in our sample, using different oxygen abundance indicators. The oxygen abundance covers the range $7.15 < 12 + \log(\mathrm{O/H}) < 9.0$, and nitrogen is found to be mostly a product of secondary nucleosynthesis for $12 + \log(\mathrm{O/H}) > 8.2$ and apparently a product of primary nucleosynthesis for $12 + \log(\mathrm{O/H}) < 8.2$. To assess the possible systematic differences among different oxygen abundance indicators, we have compared oxygen abundances of BCGs obtained with the T_e method, R_{23} method, P method, N2 method and O3N2 method. The oxygen abundances derived from the T_e method are systematically lower by 0.1−0.25 dex than those derived from the strong line empirical abundance indicators, consistent with previous studies based on H II region samples. We confirm the existence of the metallicity-luminosity relation in BCGs over a large range of abundances and luminosities. Our sample of galaxies shows that the slope of the metallicity-luminosity relation for the luminous galaxies (∼−0.05) is slightly shallower than that for the dwarf galaxies (∼−0.17). An offset was found in the metallicity-luminosity relation of the local galaxies and that of the intermediate redshift galaxies. It shows that the metallicity-luminosity relation for the emission line galaxies at high redshift is displaced to lower abundances, higher luminosities, or both.

Key words. galaxies: abundances – galaxies: starburst – stars: formation

1. Introduction

Spectra of BCGs are dominated by the emission of young, hot star clusters that ionize their environment, and are characterized by their blue color, compact appearance, high gas content, strong nebular emission lines and low chemical abundances (Kunth & Östlin 2000; Stasińska et al. 2001). Recent analyses of such objects, comparing the observed nebular emission lines, colors and stellar features with population synthesis models, found that most have experienced a recent, quasi-instantaneous burst of star formation (Mas-Hesse & Kunth 1999; Noeske et al. 2000; Kong 2004). In addition, there is ample evidence for older stellar populations in BCGs (Thuan 1983; Papaderos et al. 1996; Kong et al. 2003; Noeske et al. 2003).

Metallicity is a key parameter that controls many aspects in the formation and evolution of galaxies. The metallicity of BCGs is a parameter of recognized importance when trying to characterize their evolutionary status and link them to other objects showing overlapping properties, like dwarf irregular, low surface brightness galaxies, or high redshift compact galaxies (Hunter & Hoffman 1999; Contini et al. 2002; Izotov et al. 2004). Metal content is also at the base of global relations like those existing or searched for with the luminosity and the gas mass fraction (Pérez-Montero & Díaz 2003; Kennicutt et al. 2003). Undergoing intense bursts of star formation, strong and narrow emission line spectra, relative small dust extinction, low metal environments and different star formation histories make BCGs appropriate laboratories to study the metallicity of galaxies (Kunth & Östlin 2000). We have undertaken an extensive long-slit spectral observation of BCGs. In the papers of this series, we have studied the stellar populations, star formation histories and star formation rates of BCGs. In the present paper, we determined the oxygen abundance for 72 star-forming BCGs in our sample, based on our high quality ground-based spectroscopic observations.

The determination of oxygen abundance is a critical stage prior to deriving the value for the metallicity in galaxies and the abundances for several other elements. The preferred method for determining the oxygen abundance in galaxies using H II regions is through electron temperature-sensitive lines (the so-called T_e method), such as the [O III]λ4363 line (Kennicutt et al. 2003). However, for oxygen-rich galaxies, the oxygen line [O III]λ4363 is weak and difficult to detect. Alternative abundance determinations consist of empirical calibrations of

the strong emission lines which are easily observable, such as the R_{23} method, P method, N2 method and O3N2 method (Pagel et al. 1979; Kobulnicky et al. 1999; Pilyugin et al. 2001; Charlot & Longhetti 2001; Denicoló et al. 2002; Pettini & Pagel 2003; Tremonti et al. 2004). These methods are based on the direct measurements of the electronic temperature of low metallicity galaxies and on theoretical models for high metallicity galaxies, without any direct electron temperature measurement. Based on our homogeneous BCG optical spectral sample, we determined the oxygen abundance of BCGs by both the T_e method and those empirical methods. The results can be used to test the consistency of these different oxygen abundance indicators and to understand the physical origins of any systematic differences.

Interest in the relationship between luminosity (mass) and metallicity dates back several decades, begining with the seminal work of Lequeux et al. (1979). A correlation between the metallicity and the blue luminosity for irregulars, spirals and ellipticals was demonstrated by various authors (Garnett & Shields 1987; Skillman et al. 1989; Zaritsky et al. 1994; Melbourne & Salzer 2002; Lamareille et al. 2004; Tremonti et al. 2004), over ∼10 mag in luminosity and 2 dex in metallicity. However, some recent studies do not support these results for all types of galaxies. In a sample of low surface brightness galaxies, McGaugh (1994) saw no relationship between M_B and O/H. In a careful reanalysis of data using only the abundances determined from [O III]λ4363, Hidalgo-Gámez & Olofsson (1998) found no relationship between M_B and O/H of irregular galaxies. Hunter & Hoffman (1999) found that the relationship between M_B and O/H for Im, Sm and blue compact dwarf galaxies has a very large scatter. The question is whether the metallicity-luminosity relation for dwarf galaxies exists in a similar manner as for massive galaxies. Using a sample of 519 star-forming emission-line galaxies from the KPNO International Spectroscopic Survey, Melbourne & Salzer (2002) found that the slope of the metallicity-luminosity relation for luminous galaxies is steeper than that for dwarf galaxies. Using 1000 individual spectra of H II regions in 54 late-type galaxies, however, Pilyugin et al. (2004) found that the slope of the metallicity-luminosity relationship for spirals ($M_B = -18 \sim -22$) is slightly shallower than the one for irregular galaxies ($M_B = -12 \sim -18$). Using 72 star-forming BCGs ($M_B = -22 \sim -13$ mag), we will investigate the slope of the metallicity-luminosity relationship of BCGs.

We begin with a brief description of the spectroscopic observation and data reduction in Sect. 2. We outline our method for measuring electron density and temperature in Sect. 3. We determine the oxygen abundance of BCGs by different methods in Sect. 4. In Sect. 5 we compare our results with previous studies, and analyze the oxygen discrepancy between different methods, the luminosity-metallicity relation and the N/O – O/H relation of BCGs. The conclusions are summarized in Sect. 6.

2. Observations and data reduction

To study the stellar components, star formation histories, star formation rates and metallicities of BCGs, we have prepared an atlas of optical spectra of the central regions of 97 BCGs in the first paper of this series (Kong & Cheng 2002). The spectra were obtained at the 2.16 m telescope at the XingLong Station of the National Astronomical Observatory of China. A 300 line mm^{-1} grating was used to achieve coverage in the wavelength region from 3580 to 7400 Å with about 4.8 Å per pixel resolution. The emission line equivalent widths and fluxes for our BCG sample were provided in the second paper of this series (Kong et al. 2002). The typical uncertainties of the measurements are less than 10% for Hα6563, Hβ4861, and [O II] emission lines. The fluxes were dereddened for Galactic extinction, using the extinction coefficients from Schlegel et al. (1998) and the empirical extinction law from Cardelli et al. (1989).

To derive equivalent widths for underlying stellar absorption lines and to correct the measured Balmer emission line fluxes for these absorptions, we have applied an empirical population synthesis method to our BCG spectra (Kong et al. 2003). Intrinsic reddenings (attenuation of interstellar dust) were determined using the two strongest Balmer lines, Hα/Hβ (Galactic extinction and underlying stellar absorption were corrected), and the effective absorption curve $\tau_\lambda = \tau_V(\lambda/5500\ \text{Å})^{-0.7}$, which was introduced by Charlot & Fall (2000). Using these intrinsic reddening values, the internal extinction of each galaxy was corrected. The resulting emission line fluxes, which are corrected for the underlying stellar absorption as well as Galactic and internal extinction, will be used to determine the physical conditions (electron density, temperature, oxygen and nitrogen abundance) of the galaxies in the next sections.

3. Electron density and temperature

To derive oxygen element abundances with the T_e method, we adopted a two-zone photoionized H II region model (see Sect. 4.1).

The most precise method of determining the abundances of galaxies requires the detection of [O III]λ4363, an emission line that is weak and often not detected in oxygen-rich galaxies. In our spectra, [O III]λ4363 was detected in the spectra for 45 BCGs, but only 20 of them have equivalent widths for [O III]λ4363 larger than 2 Å, and uncertainties of the [O III]λ4363 flux measurements less than 20%. For these 20 BCGs, the electron temperature T_e(O III) of the ionized gas was calculated using the method outlined by Shaw & Dufour (1995) from the line flux ratio [O III]λ4363/(λ4959+λ5007). For other BCGs, where the temperature sensitive line [O III]λ4363 is undetectable or has a low signal-to-noise ratio, an empirical relation of T_e and strong spectral lines has been adopted for the electron temperature determination (Pilyugin 2001). The temperature will be used for derivation of the O^{+2} ionic abundances.

To estimate the temperature in the low-temperature zone T_e(O II), the relation between T_e(O II) and T_e(O III) from Garnett (1992) is utilized:

$$t_e(\text{O II}) = 0.7 \times t_e(\text{O III}) + 0.3, \quad (1)$$

where $t_e = T_e/10^4$ K. The temperature T_e(O II) is used to derive the O^+ ionic abundance.

Because the velocity dispersions of galaxies are typically hundreds of $\mathrm{km\,s^{-1}}$, the classical density diagnostic [O II]$\lambda\lambda$3726, 3729 lines are barely resolved, so they do not place significant constraints on the density. In this paper, the electron number density n_e of BCGs was determined by using the [S II]λ6716/λ6731 line ratio. In several cases where the sulfur lines are too noisy to accurately determine the electron density, we assume a density of 100 $\mathrm{cm^{-3}}$. This assumption almost does not affect our oxygen abundance determination, since the effect of temperature is much larger than that of electron density, which can be inferred from Eq. (4). In all cases, we assume that the density does not vary significantly from high-ionization zone to low-ionization zone. Calculations of the electron number density are carried out using a five-level statistical equilibrium model in the IRAF NEBULAR package (de Robertis et al. 1987; Shaw & Dufour 1995), which makes use of the latest collision strengths and radiative transition probabilities.

The measured electron temperatures T_e(O III), and electron number densities are presented, respectively, in the second and third columns of Table 1.

4. Determinations of oxygen abundance

4.1. T_e method

To derive the oxygen abundance of BCGs, it has been assumed that the oxygen lines originate in two regions: a high-ionization zone with the temperature T_e(O III), where [O III] lines originate; and a low-ionization zone with the temperature T_e(O II), where [O II] lines originate. From the weakness of He IIλ4686, we know that a negligible fraction of the gas is in O^{+3}, so the oxygen abundance is simply the sum (O^++O^{++}) by the expressions from Pagel et al. (1992):

$$\frac{\mathrm{O}}{\mathrm{H}} = \frac{\mathrm{O^+}}{\mathrm{H^+}} + \frac{\mathrm{O^{++}}}{\mathrm{H^+}}, \tag{2}$$

$$12 + \log(\mathrm{O^{++}/H^+}) = \log\frac{I([\mathrm{O\,III}]\lambda\lambda4959,5007)}{I(\mathrm{H}\beta)} + 6.174 + \frac{1.251}{t_e(\mathrm{O\,III})} - 0.55\log t_e(\mathrm{O\,III}), \tag{3}$$

$$12 + \log(\mathrm{O^+/H^+}) = \log\frac{I([\mathrm{O\,II}]\lambda3727)}{I(\mathrm{H}\beta)} + 5.890 + \frac{1.676}{t_e(\mathrm{O\,II})} - 0.40\log t_e(\mathrm{O\,II}) + \log(1 + 1.35x), \tag{4}$$

where n_e is the electron density in $\mathrm{cm^{-3}}$, and $x = 10^{-4} n_e t_e(\mathrm{O\,II})^{-1/2}$.

For 70 out of 72 galaxies in our sample, we have measured the oxygen abundance from the T_e method, and present them in the fourth column of Table 1. For the remaining two BCGs, III Zw 42 and I Zw 101, the [O III]λ5007 line has a too low signal-to-noise ratio for reliable flux measurements, and the oxygen abundances cannot be determined by the T_e method.

4.2. R_{23} method

The key for accurate determination of oxygen abundances in galaxies by the T_e method is a precise measurement of the weak auroral forbidden emission line [O III]λ4363. In star formation galaxies the temperature-sensitive [O III]λ4363 line intensity correlates with the overall abundance, being relatively strong in very low metallicity systems and becoming undetectable even for moderately low metallicity galaxies (e.g. metallicity higher than 0.5 solar metallicity). As a result, for most of the star formation galaxies [O III]λ4363 is unmeasurably weak (McGaugh 1991).

To overcome this problem, Pagel et al. (1979) suggested the empirical abundance indicator

$$R_{23} = \frac{I([\mathrm{O\,II}]\lambda3727) + I([\mathrm{O\,III}]\lambda\lambda4959,5007)}{I(\mathrm{H}\beta)} \tag{5}$$

for high metallicity galaxies. The method has been subsequently refined and calibrated using both observational data and models (e.g. McGaugh 1991). Kobulnicky et al. (1999) showed that it can be as precise as 0.2 dex.

A major difficulty associated with this method is that the relation between oxygen abundance and R_{23} is double valued, requiring some assumption or rough a priori knowledge of a galaxy's metallicity in order to locate it on the appropriate branch of the curve. In this work, the [N II]λ6584/Hα line ratio will be used to break the degeneracy of the R_{23} relation (Denicoló et al. 2002). The division between the upper and the lower branch of the R_{23} relation occurs around $\log([\mathrm{N\,II}]\lambda6583/\mathrm{H}\alpha) \simeq -1.26$ ($12 + \log(\mathrm{O/H}) \simeq 8.2$). We use the most recent R_{23} analytical calibrations given by Kobulnicky et al. (1999) which are based on the models by McGaugh (1991) to determine the oxygen abundances of BCGs in our sample. The computed oxygen abundances by the R_{23} method are shown in the fifth column of Table 1.

4.3. P method

New methods for abundance determinations using strong lines have been developed recently. These methods achieve a good approximation to the results obtained with the T_e method.

One of these new calibrations, the P method, was proposed by Pilyugin (2000, 2001). By comparing oxygen abundances in H II regions derived with the T_e method and those derived with the R_{23} method, the author found that the error in the oxygen abundance derived with the R_{23} method involves two parts, a random error and a systematic error. The origin of this systematic error is the dependence of the oxygen emission lines on not only the oxygen abundance, but also on the other physical conditions (hardness of the ionizing radiation and a geometrical factor).

To determine accurate abundances in HII regions and galaxies, Pilyugin derived a new relation between the oxygen abundance and the value of the abundance index R_{23}, the excitation parameter P. The best fitting relations

$$12 + \log(\mathrm{O/H})_P = \frac{R_{23} + 54.2 + 59.45P + 7.31P^2}{6.07 + 6.71P + 0.37P^2 + 0.243R_{23}} \tag{6}$$

Table 1. Electron temperatures, electron densities, oxygen abundances and nitrogen to oxygen abundances of BCGs.

Galaxy name	T_e (K)	n_e ($e^- cm^{-3}$)	O/H[1] (T_e)	O/H (R_{23})	O/H (P)	O/H (N2)	O/H (O3N2)	N/O[2]	O/H (OTH)[3]
iiizw12	9042.7	100.0[4]	8.34	8.69	8.34	8.65	8.55	−1.07	8.53[a]
haro15	9652.4	100.0[4]	8.33	8.60	8.33	8.78	8.48	−0.84	8.56[a]
iiizw33	9539.6	199.7	8.37	8.58	8.26	8.53	8.40	−1.27	
vzw155	6636.2	1545.1	8.64	8.89	8.55	8.81	8.78	−0.89	
iiizw42	0.0	209.8	0.00	0.00	0.00	8.82	0.00	0.00	
iiizw43	6412.1	182.5	8.62	8.90	8.60	8.78	8.66	−0.82	8.99[b]
iizw23	7396.1	3208.8	8.64	8.80	8.52	8.82	8.59	−0.92	8.55[c]
iizw28	9519.2	100.0[4]	8.32	8.64	8.33	8.63	8.47	−1.08	
iizw33	14 707.6	100.0[4]	7.99	8.34	8.01	8.40	8.29	−1.40	8.03[c]
iizw40	13 679.5	80.1	8.07	8.24	7.94	7.90	0.00	−1.44	8.09[c]
mrk5	12 230.3	100.0[4]	8.05	8.00	7.82	8.15	0.00	−1.36	8.04[b]
viizw153	10 843.7	281.6	8.23	8.54	8.23	8.51	8.37	−1.24	
viizw156	7827.8	135.9	8.51	8.75	8.51	8.56	8.42	−1.09	
haro1	7057.9	100.0[4]	8.53	8.85	8.52	8.57	8.58	−1.14	
mrk385	6883.9	21.0	8.55	8.86	8.54	8.85	8.70	−0.76	
mrk390	9674.0	712.9	8.35	8.61	8.28	8.58	8.45	−1.21	
zw0855	8894.7	504.2	8.43	8.65	8.41	8.49	8.35	−1.22	
mrk105	6526.7	145.4	8.62	8.89	8.62	8.71	8.59	−0.88	
izw18	21 334.8	104.7	7.15	7.45	7.34	7.61	0.00	−1.54	7.16[b], 7.20[e]
mrk402	13 301.8	100.0[4]	8.01	8.49	8.23	8.47	8.30	−1.17	
haro22	15 790.0	1112.7	7.88	8.22	8.06	8.12	0.00	−1.56	
haro23	9351.0	44.2	8.35	8.63	8.36	8.53	8.39	−1.18	8.40[d]
iizw44	6128.0	100.0[4]	8.63	8.93	8.62	8.88	8.82	−0.68	
haro2	9510.3	590.2	8.35	8.63	8.33	8.54	8.42	−1.22	8.40[e]
mrk148	9889.8	68.2	8.27	8.63	8.28	8.80	8.60	−0.88	
haro3	11 645.5	194.8	8.13	8.55	8.35	8.33	8.22	−1.29	8.25[b], 8.37[d]
haro25	8491.9	617.3	8.48	8.67	8.46	8.51	8.34	−1.16	
mrk1267	6709.0	100.0[4]	8.60	8.87	8.60	8.85	8.64	−0.69	8.51[a]
haro4	14 518.0	154.5	7.85	7.96	7.76	7.87	0.00	−1.48	7.81[b], 7.80[d], 7.80[e]
mrk169	8663.5	7001.9	8.62	8.66	8.44	8.86	8.51	−0.93	
haro27	10 841.3	182.9	8.20	8.57	8.21	8.56	8.46	−1.20	
mrk201	6330.6	602.3	8.68	8.90	8.66	8.98	8.69	−0.50	8.81[a]
haro28	12 648.8	362.3	8.10	8.46	8.11	8.52	8.40	−1.26	
haro8	11 645.5	138.4	8.12	8.56	8.38	8.25	8.18	−1.35	

1: O/H = 12 + log (O/H); 2: N/O = log (N/O); 3: OTH is the oxygen abundance of BCGs from the previous studies, derived by the T_e method. References: [a] Storchi-Bergmann et al. (1994); [b] Izotov & Thuan (2004); [c] Vacca & Conti (1992); [d] Hunter & Hoffman (1999); [e] Mas-Hesse & Kunth (1999); 4: n_e = 100 $e^- cm^{-3}$ is an assumption value.

can be adopted for oxygen abundance determinations in moderately high-metallicity HII regions and galaxies, 12 + log (O/H)≥ 8.2, with undetectable temperature-sensitive line ratios; and

$$12 + \log(O/H) = 6.35 + 1.45 \log R_3 - 3.19 \log P \quad (7)$$

can be adopted for oxygen abundance determinations in moderately low-metallicity HII regions and galaxies, with $R_3 = I([O\,III]\lambda\lambda 4959, 5007)/I(H\beta)$, and $P = R_3/R_{23}$.

The oxygen abundances of 59 BCGs have $\log[I([N\,II])\lambda 6583/I(H\alpha)] > -1.26$ (see in the next section), they seem to belong to the high metallicity branch calibration. The oxygen abundances of these 59 galaxies were calculated through Eq. (6). 11 of 72 BCGs belong to the low metallicity branch, Eq. (7) was used for their oxygen abundance calibration. III Zw 42 and I Zw 101 have very weak [O III]λ5007 emission lines; we did not determine their oxygen abundances. The oxygen abundances computed with the P method are shown in the sixth column of Table 1.

4.4. N2 method

Following the earlier work by Storchi-Bergmann et al. Kinney (1994) and by Raimann et al. (2000), Denicoló et al. (2002)

Table 1. continued.

Galaxy name	T_e (K)	n_e ($e^- cm^{-3}$)	O/H[1] (T_e)	O/H (R_{23})	O/H (P)	O/H (N2)	O/H (O3N2)	N/O[2]	O/H (OTH)[3]
haro29	15 407.9	151.8	7.85	8.02	7.80	7.70	0.00	−1.54	7.81[b], 7.84[d], 7.80[e]
mrk213	6445.0	1138.0	8.72	8.88	8.71	9.03	8.65	−0.37	
mrk215	6547.2	50.6	8.57	8.90	8.55	8.84	8.78	−0.78	
haro32	9842.9	26.1	8.29	8.62	8.30	8.60	8.45	−1.12	
haro33	11 363.7	1075.8	8.28	8.43	8.17	8.29	8.21	−1.57	
haro34	6467.8	473.5	8.60	8.90	8.56	8.78	8.73	−0.89	
haro36	9424.0	100.0[4]	8.37	8.61	8.37	8.31	8.27	−1.45	8.42[d]
haro35	8026.5	29.6	8.47	8.74	8.47	8.57	8.45	−1.11	
haro37	8075.5	100.0[4]	8.46	8.75	8.46	8.64	8.49	−1.04	
mrk57	8284.5	100.0[4]	8.41	8.75	8.41	8.73	8.59	−0.96	
mrk235	6624.8	243.9	8.60	8.88	8.58	8.73	8.64	−0.90	
mrk241	5918.3	98.8	8.65	8.95	8.64	8.79	8.73	−0.80	
izw53	6831.4	100.0[4]	8.59	8.86	8.58	8.74	8.60	−0.86	
izw56	8383.4	392.0	8.41	8.74	8.39	8.94	8.71	−0.57	
haro38	13 679.5	100.0[4]	8.02	8.23	8.10	8.18	8.14	−1.53	
mrk275	8797.0	2400.9	8.49	8.67	8.41	8.56	8.40	−1.24	
haro39	10 317.9	950.7	8.30	8.57	8.28	8.25	8.26	−1.62	
haro42	13 442.2	135.9	7.98	8.52	8.33	8.38	8.22	−1.15	
haro43	8744.2	4734.7	8.56	8.67	8.42	8.46	8.36	−1.52	
haro44	13 489.4	100.0[4]	8.02	8.21	8.07	8.18	8.13	−1.51	
iizw70	15 087.8	160.2	7.69	7.80	7.69	8.07	8.14	−1.38	8.00[e]
iizw71	10 900.2	203.7	8.24	8.52	8.24	8.64	8.41	−1.06	
izw97	7478.8	100.0[4]	8.51	8.80	8.51	8.66	8.54	−1.01	
izw101	0.0	100.0[4]	0.00	0.00	0.00	8.61	0.00	0.00	
izw117	6902.8	193.9	8.55	8.87	8.53	8.74	8.67	−0.93	
izw123	15 035.1	144.8	7.86	8.07	7.86	8.16	0.00	−1.29	8.46[a], 8.10[b]
mrk297	9007.4	75.1	8.34	8.69	8.35	8.69	8.56	−1.01	
izw159	12 621.6	3267.1	8.12	8.54	8.31	8.38	8.26	−1.37	
izw166	9175.6	77.1	8.37	8.64	8.37	8.57	8.41	−1.12	8.47[a]
mrk893	11 263.6	468.2	8.19	8.54	8.19	8.64	8.47	−1.10	
izw191	6306.9	100.0[4]	8.60	8.92	8.58	8.81	8.77	−0.82	
ivzw93	9993.0	1279.2	8.35	8.58	8.31	8.31	8.27	−1.54	
mrk303	7612.3	100.0[4]	8.48	8.80	8.48	8.85	8.76	−0.77	
zw2220	7116.7	224.9	8.55	8.83	8.54	8.80	8.62	−0.80	
mrk314	10 946.7	100.0[4]	8.26	8.49	8.25	8.35	8.24	−1.39	
ivzw142	7041.9	100.0[4]	8.55	8.85	8.54	8.85	8.64	−0.75	
ivzw149	9855.7	491.9	8.32	8.60	8.31	8.64	8.44	−1.07	8.48[a]
zw2335	8164.4	6515.8	8.66	8.75	8.44	8.67	8.53	−1.26	8.65[d]

focused attention on the N2 $\equiv \log[I([\mathrm{N\,II}]\lambda6583)/I(\mathrm{H}\alpha)]$ index. They collected a representative sample of spectroscopic measurements of star forming galaxies covering a wide range in metallicity ($7.2 \leq 12 + \log(\mathrm{O/H}) \leq 9.1$) from the literature, and recalculated oxygen abundances in a self-consistent manner with a precision of ∼0.2 dex.

The N2 and the oxygen abundance are well correlated (linear correlation coefficient of 0.85) and a single slope is capable of describing the whole metallicity range, from the most metal-poor to the most metal-rich galaxies in the sample. Least squares fits to the data simultaneously minimizing the errors in both axes give

$$12 + \log(\mathrm{O/H}) = 9.12 + 0.73 \times \mathrm{N2}. \quad (8)$$

Because the N2 vs. metallicity relation is monotonic, and the N2 line ratio does not depend on reddening corrections or flux

calibration, the N2 indicator was used to determine the oxygen abundance for our BCGs, and also to break the degeneracy of the R_{23} − (O/H) (in Sect. 4.2) and the P − (O/H) (in Sect. 4.3) relation. The measured oxygen abundances for BCGs by the N2 method are shown in the seventh column of Table 1.

4.5. O3N2 method

Alloin et al. (1979) was the first to introduce the quantity O3N2 ≡ log{[I([O III]λ5007)/I(Hβ)]/I([N II]λ6583)/I(Hα)]}[1], but since then the O3N2 index has been comparatively neglected in nebular abundance studies (Pettini & Pagel 2004).

Pettini & Pagel (2004) reconsidered the O3N2 vs. metallicity relation, using 137 extragalactic H II regions. The sample is similar to that of Denicoló et al. (2002). They found that at O3N2 ≤ 1.9, there appears to be a relatively tight, linear and steep relationship between O3N2 and log (O/H). A least squares linear fit to the data in the range −1 < O3N2 < 1.9 yields the relation:

$$12 + \log(\mathrm{O/H}) = 8.73 - 0.32 \times \mathrm{O3N2}. \quad (9)$$

This relationship is valid only when O3N2 ≤ 1.9. 61 out of the 72 BCGs in our sample satisfy this condition, and the oxygen abundances are estimated from the O3N2 indicator, and are shown in the eighth column of the Table 1.

5. Discussions

5.1. Oxygen abundance uncertainties

The error of the value of oxygen abundances derived with the T_e-based method and the strong line empirical methods involves two parts: a random error and a systematic error.

The main source of random errors in the oxygen abundance determination is the uncertainty in the intensities of the lines used to derive the abundances. Since we have corrected the effect of the underlying stellar absorption (by an empirical population synthesis method) and the dust extinction accurately, these effect can be neglected. The typical uncertainties of the measurements are less than 10% for most of the emission lines. Using the error of the line fluxes and standard formulae of propagation of errors, we estimate the corresponding random errors of the oxygen abundances for our galaxies. The typical error in the oxygen abundances is 0.17 dex, 0.11 dex, 0.08 dex; 0.06 dex and 0.06 dex by the T_e method, R_{23} method, P method, N2 method and O3N2 method, respectively. The typical systematic error, using the scatter of the calibrations from the respective literature, in the oxygen abundances by the T_e method is less than 0.1 dex, and is ∼0.2 dex by the strong line empirical methods.

The other uncertainty of oxygen abundances from the R_{23} method and the P method is the double-value relation between oxygen abundance and R_{23}. To break this degeneracy, the N2 = [N II]λ6584/Hα line ratio was used to discriminate between the high- and low-metallicity ranges of the P and R_{23} method calibrations. Given the scatter of the N2 vs. O/H relation, objects close to N2 = −1.26 may be either in the high or low metallicity branch of the P and R_{23} calibrations. When analyzing the galaxies in our sample, we found most of them have high or low metallicity, only 6 of them close to N2 = −1.26. Therefore, the double-value relation between oxygen abundance and R_{23} does not affect the oxygen abundances from the R_{23} and the P method for the most galaxies in our sample.

[1] This definition is slightly different from the original one proposed by Alloin et al. (1979) who included both [O III] doublet lines in the numerator of the first ratio.

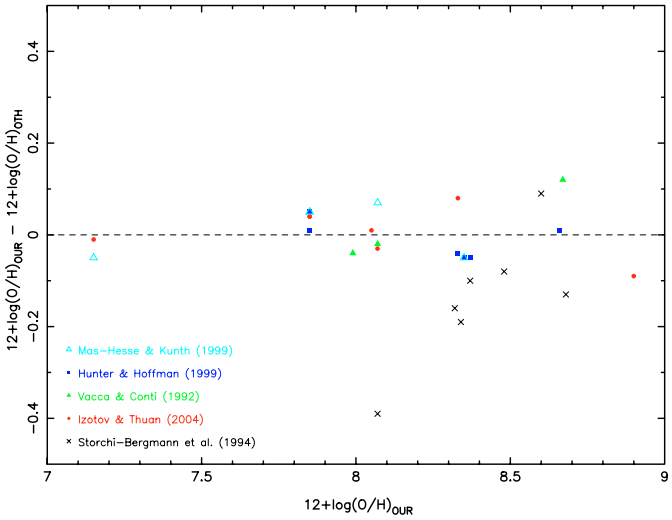

Fig. 1. Comparison of the oxygen abundances in our work with those in previous studies. The oxygen abundances were derived from the T_e-method. Filled triangles, crosses, filled squares, open triangles, and filled circles represent galaxies from Vacca & Conti (1992), Storchi-Bergmann et al. (1994), Hunter & Hoffman (1999), Mas-Hesse & Kunth (1999), and Izotov & Thuan (2004), respectively. The dashed line is the equal-value line.

5.2. Comparison with previous studies

In the last section, we have determined the oxygen abundance of BCGs in our sample, using different oxygen abundance indicators. In this section, we will discuss the differences between the results from these oxygen abundance indicators and the absolute magnitude-oxygen abundance relationship. Before this, it will be useful to compare the oxygen abundance determined from the T_e method in this work and in previous studies.

For 20 out of 72 star-forming BCGs in our sample, T_e-based oxygen abundance have been estimated in previous studies. These oxygen abundances are shown in the last column of the Table 1. The differences between the oxygen abundance estimated in our work, 12 + log (O/H)$_{\rm OUR}$, and those in other studies, 12 + log (O/H)$_{\rm OTH}$, are shown in Fig. 1 with different symbols. The oxygen abundance in our work is in good agreement with the value of Vacca & Conti (1992), Hunter & Hoffman (1999), Mas-Hesse & Kunth (1999), and Izotov & Thuan (2004), the differences are usually less than 0.1 dex. However, the discrepancy between the oxygen abundances in our work and those in Storchi-Bergmann et al. (1994) is large. One possible reason for this discrepancy are the different observation aperture sizes, a relatively large aperture (10″ × 20″)

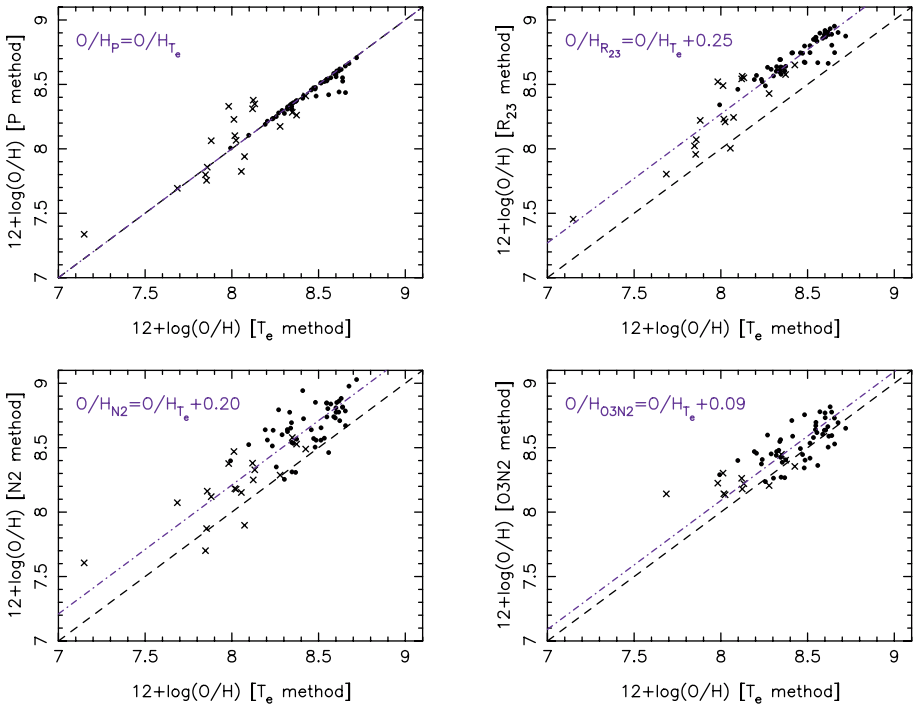

Fig. 2. Comparison of the electron temperature based abundances with those derived from different strong line calibrations. Filled circles represent galaxies with temperatures determined from the strong spectral lines (Pilyugin 2001), while crosses are used for galaxies with temperatures determined from the temperature sensitive line [O III]λ4363. The four panels show the empirical abundances using the calibrations of the P method (Pilyugin 2000; 2001), R_{23} method (Kobulnicky et al. 1999), N2 method (Denicoló et al. 2003) and O3N2 method (Pettini & Pagel 2004). The dashed line is the equal-value line, and the dot-dashed line is the best fitting linear relationship, where the fit was forced to have the same slope (equal to 1) as the equal-value line and was allowed to vary only by a constant, $O/H_{XXX} = O/H_{T_e}$ + OFFSET, O/H = 12 + log (O/H), which can be found in the upper-left corner of each panel.

having been used in Storchi-Bergmann et al. (1994) and a small slit aperture (slit width ~2″) in our work and in Vacca & Conti (1992), Hunter & Hoffman (1999), Mas-Hesse & Kunth (1999) and Izotov & Thuan (2004), if there exists a radial metallicity gradient or line flux/ionization gradient in BCGs.

5.3. Oxygen abundance from different indicators

Abundance estimates based on the strong line empirical methods have largely supplanted the direct, T_e-based determinations for large-scale abundance surveys and cosmological look-back studies. With the large range in oxygen abundance in our BCG sample, it is instructive to study the difference of the oxygen abundance from the T_e-based method and from the empirical determination methods.

Figure 2 shows the plot of the T_e-based oxygen abundance against the empirical method oxygen abundances for the blue compact galaxies in our sample. Galaxies with temperatures determined from the temperature sensitive line [O III]λ4363 are presented as crosses, and those with temperatures from the strong spectral lines (following Pilyugin et al. 2001, see Sect. 3 of this paper) are presented as filled circles. Both abundances with temperatures determined from the [O III]λ4363 and from the strong spectral lines are regarded as the standard T_e-based abundance and used to study the offset between the P-, R_{23}-, N2-, O3N2-method abundances and the T_e-based abundances.

It shows that although with a large scatter, there is an agreement between the oxygen abundance from the T_e method and those from the empirical methods for these low metallicity galaxies whose temperatures are determined from the [O III]λ4363 line. But for high metallicity galaxies, there exists an offset between the oxygen abundance from the empirical methods and the T_e-based method.

Figure 2a shows that there is a good agreement between the O/H_{T_e} and the O/H_P abundances for high metallicity galaxies. Because the temperature of these high metallicity galaxies was determined by the P method too (Pilyugin 2001), this agreement can be understood easily, and cannot be used to test the validity of the P method. For the other indicators, although all the T_e-based galaxy abundances trace a locus which is roughly consistent in shape with the empirical calibrations, there is a pronounced offset in abundance in most cases, as has been pointed out previously (Stasińska 2002; Kennicutt et al. 2003). In all cases, the empirical calibrations yield oxygen abundances that are systematically higher than the T_e-based abundances, by amounts ranging from 0.09 to 0.25 dex on average. The systematic offset may have significant consequences for the nebular abundance scale as a whole. If the T_e abundances are correct, it implies that most studies of the galactic abundances (locally and at high redshift) based on empirical nebular line calibrations have over-estimated the true absolute oxygen abundances by factors of 1.2−1.8 for high metallicity galaxies, as was noted by Kennicutt et al. (2003).

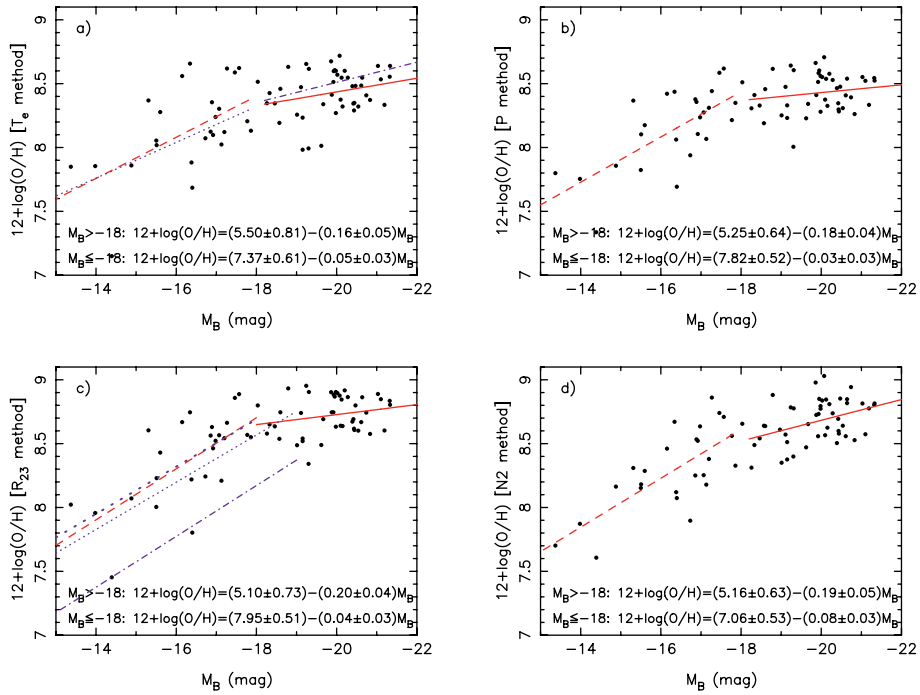

Fig. 3. Luminosity-metallicity relations for BCGs in our sample, the oxygen abundances were derived from methods in Sect. 4. The solid line is a linear least squares fit to the luminous galaxies ($M_B \leq -18$), the dashed line is a linear least squares fit to the dwarf galaxies ($M_B > -18$, blue compact dwarf galaxies). The dotted and dash-dotted lines in **a)** show the relation from Pilyugin et al. (2004a) for the irregular and spiral galaxies. The dotted line in **c)** shows the relation for about 50 000 SDSS star-forming galaxies from Tremonti et al. (2004), the thick-dotted line in **c)** shows the best fitting line for our dwarf galaxies with the same slope as Tremonti et al. (2004), but with different offset, and the dash-dotted lines in **c)** shows the relation of the intermediate redshift galaxies from Maier et al. (2004).

The discrepancies shown in Fig. 2 can be traced to two main origins, an insufficient number of calibrating H II regions with accurate T_e-based abundances in the earliest calibrations of the empirical methods and a systematic offset between the nebular electron temperatures in the calibrating photoionization models and the observed forbidden-line temperatures for a given strong line spectrum (Kennicutt et al. 2003). Detailed discussions of the reasons of these discrepancies can be found in Kennicutt et al. (2003).

Currently, we cannot be certain whether the discrepancies in abundance scales are due to the biases in the T_e-based results, or the problems in the theoretical models that are used to calibrate most of the strong line empirical abundance indicators. High-quality far-infrared measurements of a sample of extragalactic HII regions, including some of the principal fine-structure cooling lines, may help to resolve these inconsistencies.

5.4. The luminosity-metallicity relationship

Using different oxygen abundance indicators, the oxygen abundances of BCGs have been determined in the last section. Combining oxygen abundance and absolute magnitude of galaxies, we can study the luminosity-metallicity relationship of BCGs.

Figure 3 shows the absolute magnitude M_B (Kong & Cheng 2002a) vs. oxygen abundance relation for BCGs in our sample. The general trend, widely discussed in the literature and confirmed here, is an increase of metallicity with luminosity over a large magnitude range, from $M_B = -13$ to -22. We also found that there is not a tight correlation between the two quantities. The origin of this scatter may be due to the differences in the star formation history, the evolutionary status of the current starburst, different initial mass function, starburst-driven outflows, winds, gas infall or due to the errors in metallicity determination. In addition, the relationship for the luminous galaxies ($M_B \leq -18$) is shallower than that of the dwarf galaxies ($M_B > -18$).

To check any dependency of the luminosity-metallicity relation on the choice of the O/H calibration, the oxygen abundances determined by the T_e, P, R_{23}, and N2 methods were plotted in the different panels of Fig. 3 (the abundance from the O3N2 method is not used, since this method does not work well for low metallicity dwarf galaxies). In each case, we performed a linear regression on the luminosity-metallicity relation for the luminous galaxies ($M_B \leq -18$) and the dwarf galaxies ($M_B > -18$). We does not consider the errors of M_B and the fits were weighted by the errors of the O/H data. The solid line is the luminosity-metallicity relation for the luminous galaxies, and the dashed line is the best fitting line for the dwarf galaxies. We found that the slopes of the different luminosity-metallicity relations are similar; the choice of oxygen indicator has a small effect on the slope of the luminosity-metallicity relation. However, the different methods for oxygen abundances determined can introduce zeropoint differences in the luminosity-metallicity relations.

It is instructive to compare our determination of the luminosity-metallicity relation with other published determinations, both to validate the consistency of our measurements and to compare the luminosity-metallicity relation in the different types of galaxies. In Fig. 3a, we plot the luminosity-metallicity relation for the spiral galaxies (dot-dashed line)

$$12 + \log(\mathrm{O/H})_P = (6.93 \pm 0.37) - (0.079 \pm 0.018) \times M_B(M_B < -18), \quad (10)$$

and for the local irregulars (dotted line)

$$12 + \log(\mathrm{O/H})_P = (5.80 \pm 0.17) - (0.139 \pm 0.011) \times M_B(M_B > -18), \quad (11)$$

derived by Pilyugin et al. (2004a). Inspection of Fig. 3a shows that the luminosity-metallicity relationship for BCGs in our sample agrees, within the uncertainties, with that from Pilyugin et al. (2004a). We confirm the existence of the difference of the slopes for the luminosity-metallicity relationships between luminous and dwarf galaxies.

Using a sample of 53 400 star-forming galaxies at $z \sim 0.1$ in the Sloan Digital Sky Survey, Tremonti et al. (2004) derived a luminosity-metallicity relation

$$12 + \log(\mathrm{O/H}) = (5.238 \pm 0.018) - (0.185 \pm 0.001) \times M_B \quad (12)$$

for nearby galaxies ($M_B > -21$ mag) using the new techniques that make use of the approach outlined by Charlot et al. (in preparation). This consists of estimating metallicity statistically, based on simultaneous fits of all the most prominent emission lines ([O II], Hα, [O III], Hβ, [N II], [S II]) with a model designed for the interpretation of integrated galaxy spectra (Charlot & Longhetti 2001). This relation was plotted in Fig. 3c as a dotted line. Figure 3c shows that the slope of Tremonti et al. (2004) is almost same as that of ours, but there is a small offset between the curves. The small offset can be derived by fitting lines with a slope forced to the value by Tremonti et al. (2004). As a result, our new luminosity-metallicity relation becomes

$$12 + \log(\mathrm{O/H})_{R_{23}} = (5.36 \pm 0.72) - 0.185 \times M_B(M_B > -18), \quad (13)$$

and is presented in Fig. 3c as a thick-dotted line. A zeropoint offset, $\Delta\log(\mathrm{O/H}) \sim 0.12$, between Tremonti et al. (2004) and ours was found. The method differences should not induce this offset because the R_{23} method and the method used by Tremonti et al. (2004) are both based on the similar strong lines. The different redshift range in our sample ($z \sim 0.0$) and that in Tremonti et al. (2004) ($z \sim 0.1$) may cause this offset. However, the significance is not very high (see the errors in Eq. (13)). To further assess this possible trend with redshift, we also plotted the luminosity-metallicity relation

$$12 + \log(\mathrm{O/H})_{R_{23}} = (4.59 \pm 0.91) - (0.20 \pm 0.046) \times M_B(M_B > -19), \quad (14)$$

for emission line galaxies at intermediate redshifts ($z \simeq 0.4$) in Fig. 3c as dashed-dotted line (Maier et al. 2004). A larger zeropoint offset, $\Delta\log(\mathrm{O/H}) \sim 0.51$, was found for these intermediate redshift galaxies.

Comparison between the luminosity-metallicity relationships in the different redshift ranges shows that the luminosity-metallicity relation at high redshift is displaced to lower abundance and higher luminosities compared to today. One explanation could be that intermediate-redshift galaxies are slightly less advanced in their evolution and, as a consequence, are slightly more metal-deficient than local galaxies of the same luminosity. As an alternative, intermediate-redshift galaxies may have just undergone a powerful starburst which temporarily increases their blue luminosity (Pilyugin et al. 2004b).

5.5. The N/O versus O/H relationship

The origin of nitrogen has been a subject of debate for some years. Nitrogen is thought to be synthesized in the CNO process during hydrogen burning. However the stars responsible remain uncertain (Izotov & Thuan 1999, for short as IT99; Kunth & Östlin 2000; Contini et al. 2002). In the case of *secondary* synthesis, oxygen and carbon have been produced in the previous generations of stars, and the nitrogen, produced in the present generation of stars, should be proportional to their initial heavy element abundance. Secondary nitrogen production is expected in stars of all masses (see IT99). In the case of *primary* nitrogen synthesis, on the other hand, oxygen and carbon are produced in the same stars prior to the CNO cycle rather than in previous generations, and nitrogen production should be independent of the initial heavy element abundance. Primary nitrogen production is thought to occur mainly in intermediate-mass stars, yet important contributions may also come from high mass stars (see for example Weaver & Woosley 1995; IT99; Izotov et al. 2004, and references therein). Therefore, the N/O abundance ratio as a function of the O/H ratio is a key relation for understanding the origin of nitrogen of galaxies.

To understand the origin of nitrogen in BCGs, we plot the distributions of $12 + \log(\mathrm{O/H})$ and $\log(\mathrm{N/O})$ abundance ratios for our sample galaxies in Fig. 4. The N/O abundance ratios in BCGs were determined from the expression (Pagel et al. 1992):

$$\log(\mathrm{N/O}) = \log(\mathrm{N^+/O^+}) = \log\frac{I([\mathrm{N\,II}]\lambda\lambda 6548, 6584)}{I([\mathrm{O\,II}]\lambda 3727)} + 0.31 - \frac{0.726}{t_e([\mathrm{N\,II}])} - 0.02\log t_e([\mathrm{N\,II}]) - \log\frac{1 + 1.35x}{1 + 0.12x}, \quad (15)$$

where $t_e([\mathrm{N\,II}]) = t_e([\mathrm{O\,II}])$, and $x = 10^{-4} n_e t_e([\mathrm{N\,II}])^{-1/2}$. Fitting lines, based on the solar neighborhood dwarf stars, from Tomkin & Lambert (1984) for a primary (dashed line), and a secondary (dot-dashed line) production of nitrogen are shown in Fig. 4 too.

To show the dependence of the relation between N/O and O/H on the methods for determining oxygen abundance, the oxygen abundances determined by both the T_e-based method and the strong line empirical abundance methods are shown in Fig. 4. It should be noted that O/H from methods based on [N II] line (such as the N2 and the O3N2 methods) are suspicious because these O/H are empirical and

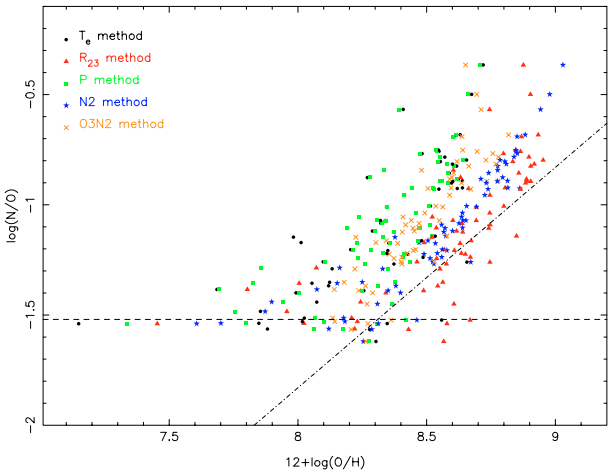

Fig. 4. Logarithm of the number ratio of nitrogen to oxygen abundances plotted against 12 + log (O/H). Different symbols represent oxygen abundances from different methods, as shown in the upper-left corner of the figure and in Sect. 4. The dashed line (*primary* origin) and the dot-dashed line (*secondary* origin) represent the mean relation for galactic dwarf stars (Tomkin & Lambert 1984). The points are not corrected for the mean O/H offsets derived for the different O/H calibrators in Sect. 5.3.

nitrogen-dependent. Therefore, we draw conclusions from the T_e, P, R_{23} method, which should be independent of nitrogen.

In our sample, only one galaxy, I Zw 18, has a very low metallicity, 12 + log (O/H) < 7.6, and the log (N/O) of I Zw 18 is about −1.5, which is consistent with that in IT99 and references therein, and the fitting lines from Tomkin & Lambert (1984) for a primary production of nitrogen. For galaxies with moderately low metallicity, 7.6 < 12 + log (O/H) < 8.2, Fig. 4 shows that the N/O ratio begins to increase with the oxygen abundance above ∼−1.50 along with the scatter. For galaxies with 12 + log (O/H) < 7.6, IT99 interpreted these results as primary nitrogen production by massive stars only. In this scenario, galaxies in that O/H range are young, so that primary nitrogen from intermediate mass stars has not been released yet. Only in slightly older galaxies, do intermediate-mass stars start to contribute secondary nitrogen, leading to the higher mean and scatter of N/O ratios seen for 7.6 < 12 + log (O/H) < 8.2. For an alternative interpretation, see e.g. Izotov et al. (2004) and references therein. For the galaxies with high metallicity, 12 + log (O/H) > 8.2, the N/O ratio increases with the oxygen abundance more rapidly, indicating that, in this metallicity regime, nitrogen is primarily a *secondary* element, and the contribution from the primary production is not important. The dispersion of N/O scatter is roughly about ±0.3 dex. This scatter looks similar to that obtained by IT99.

6. Summary and conclusions

We determined the electron temperatures, electron densities, nitrogen abundance and oxygen abundance for 72 star-forming blue compact galaxies in our sample, using different oxygen abundance indicators. The discrepancies of the oxygen abundances from different indicators, the relations between the oxygen abundance and luminosity and the N/O vs. O/H were investigated. We obtained the following results.

1. The oxygen abundance in our BCGs ranges from 12 + log (O/H) = 7.15 to 9.0. The oxygen abundance derived from the T_e-based method in our work is in good agreement with the values of previous studies; the differences between them are usually less than 0.1 dex where observed aperture sizes are comparable.
2. To study how significantly the oxygen abundance depends on the derivation method, the oxygen abundance of BCGs was measured with the T_e-based method and the strong line empirical abundance methods (such as the R_{23}, P, N2 and O3N2). We found that the empirical calibrations yield oxygen abundances that are systematically higher than the T_e-based abundances, by amounts ranging from 0.09 to 0.25 dex on average.
3. We have confirmed the existence of the metallicity-luminosity relation in BCGs. It shows that the slope of the metallicity-luminosity relation for the luminous galaxies ($M_B < -18$) is shallower than that for the dwarf galaxies($M_B > -18$), and the metallicity-luminosity relation for emission line galaxies at high redshift is displaced to lower abundances, higher luminosities, or both, compared to BCGs in the local Universe.
4. The relation between the N/O and the O/H abundance ratios from our data confirms the results of previous work (IT99). In the high metallicity regime, 12 + log (O/H) > 8.2, nitrogen is primarily a secondary element. For galaxies with lower metallicities, nitrogen originates mainly from primary production in intermediate and high mass stars.

Acknowledgements. We thank L. S. Pilyugin, A. C. Phillips for their helpful suggestions. The referee, K. G. Noeske, is thanked for the constructive report, which helped improve the paper. This work is based on observations made with the 2.16 m telescope of the National Astronomical Observatory of China. X.K. acknowledges support provided by the Japan Society for the Promotion of Science (JSPS).

References

Alloin, D., Collin-Souffrin, S., Joly, M., & Vigroux, L. 1979, A&A, 78, 200
Cardelli, J. A., Clayton, G. C., & Mathis, J. S. 1989, ApJ, 345, 245
Charlot, S., & Fall, S. M. 2000, ApJ, 539, 718
Charlot, S., & Longhetti, M. 2001, MNRAS, 323, 887
Contini, T., Treyer, M. A., Sullivan, M., & Ellis, R. S. 2002, MNRAS, 330, 75
de Robertis, M. M., Dufour, R. J., & Hunt, R. W. 1987, JRASC, 81, 195
Denicoló, G., Terlevich, R., & Terlevich, E. 2002, MNRAS, 330, 69
Garnett, D. R. 1992, AJ, 103, 1330
Garnett, D. R., & Shields, G. A. 1987, ApJ, 317, 82
Hidalgo-Gamez, A. M., & Olofsson, K. 1998, A&A, 334, 45
Hunter, D. A., & Hoffman, L. 1999, AJ, 117, 2789
Izotov, Y. I., & Thuan, T. X. 1999, ApJ, 511, 639
Izotov, Y. I., & Thuan, T. X. 2004, ApJ, 602, 200
Izotov, Y. I., Stasińska, G., Guseva, N. G., et al. 2004, A&A, 415, 87
Kennicutt, R. C., Bresolin, F., & Garnett, D. R. 2003, ApJ, 591, 801
Kobulnicky, H. A., Kennicutt, R. C., & Pizagno, J. L. 1999, ApJ, 514, 544

Kong, X. 2004, A&A, 425, 417
Kong, X., & Cheng, F. Z. 2002, A&A, 389, 845
Kong, X., Cheng, F. Z., Weiss, A., & Charlot, S. 2002, A&A, 396, 503
Kong, X., Charlot, S., Weiss, A., & Cheng, F. Z. 2003, A&A, 403, 877
Kunth, D., & Östlin, G. 2000, A&AR, 10, 1
Lamareille, F., Mouhcine, M., Contini, T., et al. 2004, MNRAS, 350, 398
Lequeux, J., Rayo, J. F., Serrano, A., Peimbert, M., & Torres-Peimbert, S. 1979, A&A, 80, 155
Mas-Hesse, J. M., & Kunth, D. 1999, A&A, 349, 765
Maier, C., Meisenheimer, K., & Hippelein, H. 2004, A&A, 418, 475
McGaugh, S. S. 1991, ApJ, 380, 140
McGaugh, S. S. 1994, ApJ, 426, 135
Melbourne, J., & Salzer, J. J. 2002, AJ, 123, 2302
Noeske, K. G., Guseva, N. G., Fricke, K. J., et al. 2000, A&A, 361, 33
Noeske, K. G., Papaderos, P., Cairós, L. M., & Fricke, K. J. 2003, A&A, 410, 481
Pagel, B. E. J., Edmunds, M. G., Blackwell, D. E., et al. 1979, MNRAS, 189, 95
Pagel, B. E. J., Simonson, E. A., Terlevich, R. J., & Edmunds, M. G. 1992, MNRAS, 255, 325
Papaderos, P., Loose, H.-H., Thuan, T. X., et al. 1996, A&AS, 120, 207
Pérez-Montero, E., & Díaz, A. I. 2003, MNRAS, 346, 105
Pettini, M., & Pagel, B. E. J. 2004, MNRAS, 348, L59
Pilyugin, L. S. 2000, A&A, 362, 325
Pilyugin, L. S. 2001, A&A, 369, 594
Pilyugin, L. S., Vílchez, J. M., & Contini, T. 2004a, A&A, 425, 849
Pilyugin, L. S., Contini, T., & Vílchez, J. M. 2004b, A&A, 423, 427
Raimann, D., Storchi-Bergmann, T., Bica, E., et al. 2000, MNRAS, 316, 559
Shaw, R. A., & Dufour, R. J. 1995, PASP, 107, 896
Schlegel, D. J., Finkbeiner, D. P., & Davis, M. 1998, ApJ, 500, 525
Skillman, E. D., Kennicutt, R. C., & Hodge, P. W. 1989, ApJ, 347, 875
Stasińska, G. 2002, Ionized Gaseous Nebulae, ed. W. J. Henney, J. Franco, M. Martos, & M. Peña (Mexico, DF: UNAM), Rev. Mex. Astron. Astrofis. Ser. Conf., 12, 62
Stasińska, G., Schaerer, D., & Leitherer, C. 2001, A&A, 370, 1
Storchi-Bergmann, T., Calzetti, D., & Kinney, A. L. 1994, ApJ, 429, 572
Thuan, T. X. 1983, ApJ, 268, 667
Tomkin, J., & Lambert, D. L. 1984, ApJ, 279, 220
Tremonti, C. A., Heckman, T. M., Kauffman, G., et al. 2004, ApJ, 613, 898
Vacca, W. D., & Conti, P. S. 1992, ApJ, 401, 543
Weaver & Woosley 1995, ApJ, 101, 181
Zaritsky, D., Kennicutt, R. C., & Huchra, J. P. 1994, ApJ, 420, 87